European Journal of Medicinal Chemistry 220 (2021) 113452

Contents lists available at ScienceDirect

European Journal of Medicinal Chemistry

journal homepage: http://www.elsevier.com/locate/ejmech

A novel Hsp70 inhibitor specifically targeting the cancer-related Hsp70-Bim protein-protein interaction

Ziqian Wang [a, 1], Ting Song [a, **, 1], Zongwei Guo [b], Laura B. Uwituze [a], Yafei Guo [b], Hong Zhang [b], Hang Wang [b], Xiaodong Zhang [a], Hao Pan [a], Tong Ji [a], Fangkui Yin [a], Sheng Zhou [a], Jian Dai [a], Zhichao Zhang [a, *]

[a] State Key Laboratory of Fine Chemicals, Zhang Dayu School of Chemistry, Dalian University of Technology, Dalian, Liaoning, 116024, China
[b] School of Bioengineering, Dalian University of Technology, Dalian, Liaoning, 116024, China

ARTICLE INFO

Article history:
Received 7 December 2020
Received in revised form
29 March 2021
Accepted 2 April 2021
Available online 14 April 2021

Keywords:
Hsp70 inhibitor
Hsp70-bim PPI
Cancer-related target
Antitumor candidate

ABSTRACT

Targeting cancer-related Hsp70-Bim protein-protein interactions (PPIs) offers a new strategy for the design of Hsp70 inhibitors. Herein, we discovered a novel Hsp70 inhibitor, **S1g-6**, based on the established BH3 mimetics. **S1g-6** exhibited sub-μM binding affinity toward Hsp70 and selectively disrupted Hsp70-Bim PPI. The target specificity of **S1g-6** *in situ* was validated by affinity-based protein profiling, co-immunoprecipitation, and cell-based shRNA assays. **S1g-6** specifically antagonized the ATPase activity of Hsp70 upon recruiting Bim and showed selective apoptosis induction in some cancer cell lines over normal ones through suppression of some oncogenic clients of Hsp70, representing a new class of antitumor candidates. Hsp70-Bim PPI exhibited cancer-dependent role as a potential anti-cancer target.

1. Introduction

Heat shock protein 70 (Hsp70) is an important ATP-dependent molecular chaperone that is abundantly expressed in many malignant tumors of various origins [1–4]. Hsp70 assists in the correct folding of many oncogenic proteins, playing critical roles in the growth, proliferation and apoptosis evasion of cancer cells and protects cancers from stress resulting from intrinsically misfolded proteins and extrinsic stimuli, including chemotherapy [1–4]. However, Hsp70 has also been reported as an important facilitator of many other cellular functions, both cancer-dependent and otherwise, and the expression level of Hsp70 exhibited no significant differences in cancer and normal cells, expressing doubts about the effectiveness of Hsp70 as a specific target for cancer therapy [5–8]. Therefore, the clinical application of Hsp70 inhibitors is often limited by the toxicity towards normal cells [9–11]. None of them have been clinically approved by the US Food and Drug Association.

The critical roles of Hsp70 and its homologs in cancer-related molecular mechanisms are thought to be mediated by protein-protein interactions (PPIs) between Hsp70 and a great amount of proteins, such as co-chaperones DNAJ and Bag-3, apoptosis-related proteins Bax, p53, caspase 3 and APAF-1, multiple co-chaperones Hsp90 and HOP, and so on [1–4]. Several Hsp70 inhibitors that disrupt these PPIs (Fig. 1a), including **JG-98**/**JG-231** (for Bag-3) [12,13], **MAL3-101** (for DNAJ class proteins) [14], **YK-5** (for Hsp90 and Hop) [15], **BT-44** (for caspase 3) [16], **apoptozole** (for APAF-1) [17] and **AEAC** (for oxidized GAPDH) [18], were developed to investigate their cancer-related molecular mechanisms. In this regard, specifically targeting cancer-related Hsp70-involved PPIs is an attractive strategy for Hsp70 inhibitor development, which is thought to reduce toxicity towards normal cells. For example, **JG-98** and **JG-231**, exhibited obvious selectivity for killing breast cancer cells over normal cells by specifically targeting the cancer-related Hsp70-Bag3 PPI [12,13,19].

Most recently, our work revealed that Bim, a BH3-only member of the Bcl-2 family proteins, serves as a co-chaperone for Hsp70, which modulates the folding and stabilization of many Hsp70 oncogenic substrates. In some chronic myeloid leukemia (CML) cell lines, Bim forms PPI with Hsp70, which facilitates the refolding and

* Corresponding author.
** Corresponding author.
E-mail addresses: songting@dlut.edu.cn (T. Song), zczhang@dlut.edu.cn (Z. Zhang).
[1] These authors contributed equally to this work.

https://doi.org/10.1016/j.ejmech.2021.113452
0223-5234/

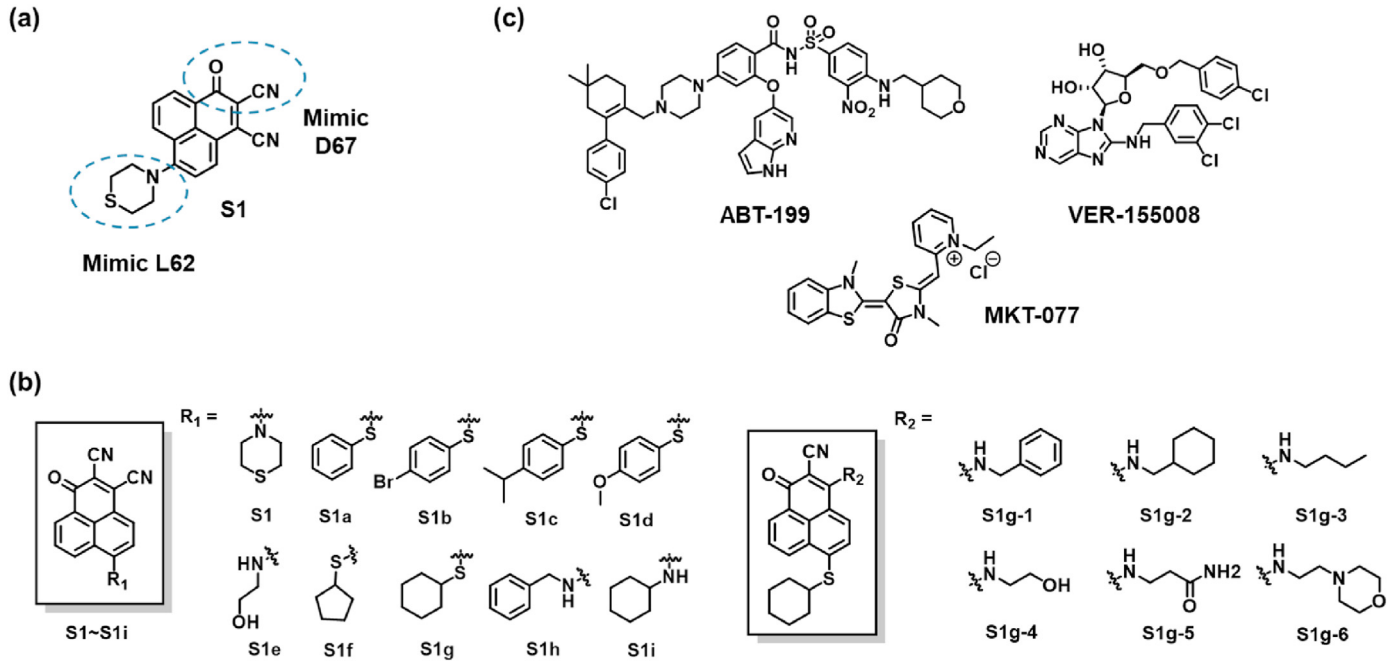

Fig. 1. (a) The chemical structure of BH3-mimetic **S1**. (b) The chemical structure of **S1~S1i** and **S1g-1~S1g-6**. (c) The chemical structure of **ABT-199**, **VER-155008** and **MKT-077**.

stabilization of many oncogenic proteins in downstream pathways of the fusion tyrosine kinase BCR-ABL, such as AKT and Raf-1, and subsequently prevent these cells from apoptosis [20].

Herein, through derivation, screening, and optimization of **S1**, a Bcl-2 inhibitor developed by our group [21,22], we discovered a novel Hsp70 inhibitor, **S1g-6**, which exhibited sub-μM binding affinity toward Hsp70 and selectively disrupted Hsp70-Bim PPI both *in vitro* and *in situ*. Compared with two well-known Hsp70 inhibitors, **VER-155008** [23] and **MKT-077** [24], that inhibit the ATPase activity of Hsp70 via competitive binding and allosteric effect, respectively, **S1g-6** exhibited stronger apoptosis induction in some CML cell lines and showed much lower cytotoxicity to normal cells, making it a completely new class of Hsp70 inhibitor and a promising antitumor candidate. With the help of **S1g-6**, Hsp70-Bim PPI could be verified as a cancer-related target.

2. Results and discussion

2.1. Rational design and synthesis

In our previous work, we revealed that Hsp70-Bim PPI is mediated by the nucleotide-binding domain (NBD) of Hsp70 and the Bcl-2 homology 3 (BH3) domain of Bim [20]. TROSY-HSQC data demonstrated that BimBH3 domain inserts into a hydrophobic groove on the surface of the NBD domain of Hsp70. Moreover, residues L62 and D67 on BimBH3 domain, two key residues for Bcl-2-Bim PPI, were also found to play critical roles on the Hsp70-Bim binding interface, indicating that the binding interface of Hsp70-Bim showed high similarity to that of Bcl-2/Bim. Therefore, we chose our previously reported BH3 mimetic (Bcl-2 inhibitor) **S1** [21,22], in which the 6-thiamorpholine and 1-carbonyl/2-cyano groups mimic the binding features of L62 and D67 on Bim, respectively, as the starting point for developing new Hsp70 inhibitors that disrupt the Hsp70-Bim PPI (Fig. 1a).

Herein, we established a library of **S1**-analogs by replacing the 6-thiamorpholine group and the 3-cyano group with a variety of different substituent groups (R_1 and R_2, Fig. 1b), in order to screen a compound that selectively fits the binding surface of Hsp70-Bim PPI over that of Bcl-2-Bim PPI. These compounds were synthesized via the route published by our group from acenaphthoquinone [21,22] (Scheme 1).

2.2. Structure-activity relationship analysis

The capability of **S1~S1i** and **S1g-1~S1g-6** to disrupt Hsp70-Bim and Bcl-2-Bim PPIs was detected via fluorescence polarization assays (FPAs) using Fam-labeled BimBH3 peptide and recombinant Hsp70 NBD (residues 1−383) and Bcl-2 (residues 2−206) protein. The well-known Hsp70 inhibitors, **VER-155008** [23] and **MKT-077** [24] (Fig. 1c), which binds distal from and adjacent to Bim-binding site, respectively, and the Bcl-2 inhibitor **ABT-199** [25], were tested in parallel (Fig. 1c). As shown in Table 1, **ABT-199** and **S1** only have the capability to disrupt Bcl-2-Bim but not the Hsp70-Bim complex (IC_{50} > 20 μM). **S1** derivatives with a thiophenol or cycloalkyl thiol group as R_1 exhibited a gain of function to disrupt the Hsp70-Bim complex (**S1a-S1d** or **S1f-S1g**), while compounds bearing amino substituents as R_1 showed weak potency in disturbing both complexes (**S1e**, **S1h** and **S1i**). Among **S1a-S1g**, compound **S1g** with a cyclohexanethiol group as R_1 exhibited a μM range of potency for disrupting Hsp70-Bim (IC_{50} = 1.7 μM) and a 5-fold selectivity to Hsp70-Bim over Bcl-2/Bim. Displacing the R_2 group of **S1g** with hydrophilic substituents, which led to **S1g-4**, **S1g-5** and **S1g-6**, compared with hydrophobic substituents **S1g-1**, **S1g-2** and **S1g-3,** further promoted the potency and selectivity to disrupt Hsp70-Bim over Bcl-2/Bim complex. Among them, **S1g-6** showed the best potency (IC_{50} = 0.45 μM) and selectivity (ratio > 40) to target Hsp70-Bim over Bcl-2/Bim. **VER-155008** shows no detetable competition to Hsp70-Bim complex, while **MKT-077** exhibited a 5-fold weaker disruption than **S1g-6.** The direct binding of **S1g-6** to Hsp70 was further verified by isothermal titration calorimetry (ITC), showing dissociation constant K_d value of 0.96 μM (Fig. 2a). Compared with the K_d = 1.78 μM of **MKT-077**, a consistent binding potency with that determined by FPA illustrated the stronger direct binding and disruption of Hsp70-Bim PPIs of **S1g-6** than **MKT-077**.

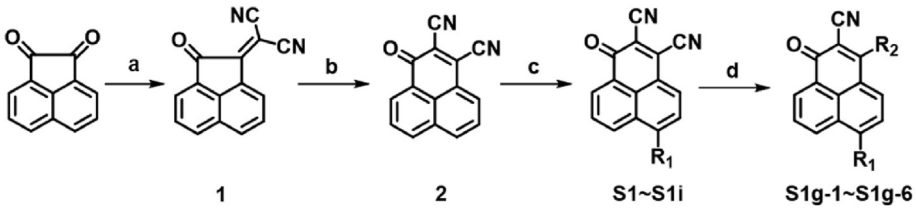

Scheme 1. Synthetic route of **S1**-analogies. Reagents and conditions: (a) malononitrile, CH_3CN, 65 °C, 3 h; (b) K_2CO_3, CH_3CN, 65 °C, 3 h; (c) R_1H, CH_3CN, 60 °C, 3 h; (d) R_2H, CH_3CN, rt, 2 h.

Table 1
The IC_{50} value of **S1~S1i** and **S1g-1~S1g-6** for disrupting Hsp70-Bim PPI and Bcl-2-Bim PPI determined by FPA.

Compounds	Hsp70-Bim IC_{50} (μM)	Bcl-2/Bim IC_{50} (μM)	Compounds	Hsp70-Bim IC_{50} (μM)	Bcl-2/Bim IC_{50} (μM)
S1	>20	0.8 ± 0.2	**S1g-1**	10.5 ± 0.1	5.2 ± 0.6
S1a	7.7 ± 1.4	1.8 ± 0.6	**S1g-2**	8.4 ± 0.5	4.8 ± 0.4
S1b	2.5 ± 0.5	0.7 ± 0.1	**S1g-3**	13.2 ± 1.8	16.0 ± 2.7
S1c	4.4 ± 1.2	2.8 ± 0.4	**S1g-4**	0.81 ± 0.27	9.6 ± 1.4
S1d	4.5 ± 0.5	6.1 ± 0.3	**S1g-5**	1.0 ± 0.3	13.5 ± 1.5
S1e	15.2 ± 2.7	>20	**S1g-6**	0.45 ± 0.10	18.7 ± 2.3
S1f	3.2 ± 0.3	8.4 ± 1.2	**ABT-199**	>20	<0.1
S1g	1.7 ± 0.5	8.6 ± 2.4	**VER-155008**	>20	>20
S1h	18.5 ± 1.9	14.8 ± 3.1	**MKT-077**	2.7 ± 0.6	>20
S1i	>20	>20			

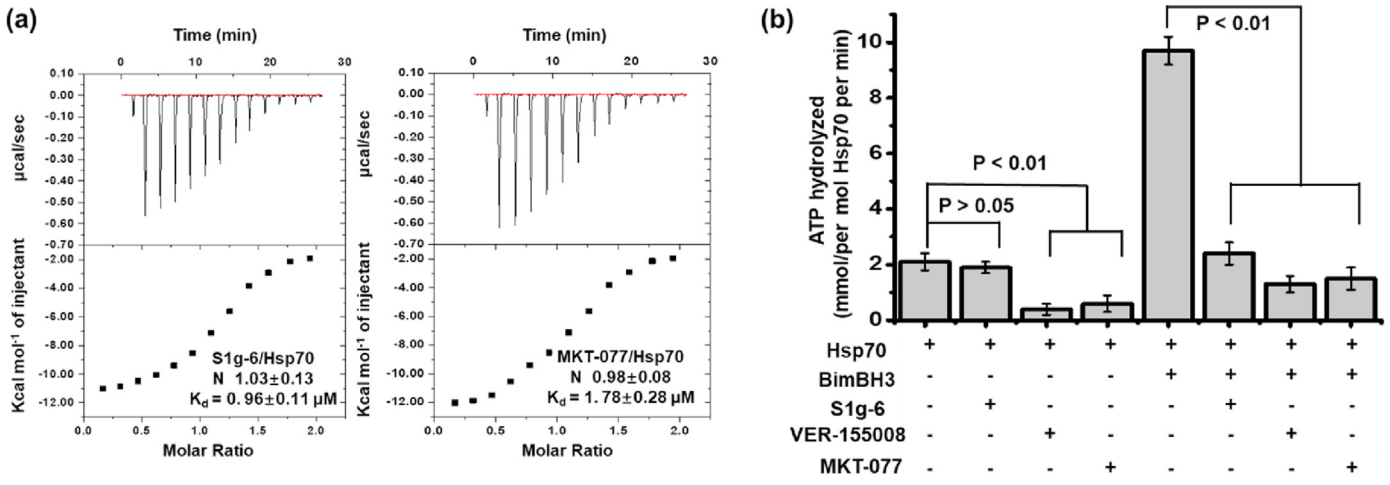

Fig. 2. (a) Binding affinity of **S1g-6** and **MKT-077** to Hsp70 determined by ITC. Data are from three independent experiments. (b) ATPase activity of Hsp70 treated with BimBH3, **S1g-6**, **VER-155008** and **MKT-077**. Error bars show the mean ± s.e.m. (n = 3).

Consequently, the single-turnover ATPase rates of Hsp70 upon the addition of **S1g-6** were detected, using **VER-155008** [23] and **MKT-077** [24] as control (Fig. 2b). The rate of ATPase activity of Hsp70 was significantly increased (4.8 fold) by synthetical BimBH3 peptide, which is consistent with the results in our published work. Notably, **S1g-6** significantly suppressed the BimBH3-stimulated ATPase activity, with no obvious influence on basal ATPase activity. On the contrary, **VER-155008** and **MKT-077** indiscriminately suppressed the ATPase activity of Hsp70 in the presence and absence of BimBH3 peptide. These data verified that **S1g-6** selectively inhibits the co-chaperone function of Bim to activate the ATPase activity of Hsp70, rather than directly suppressing the overall ATPase activity of Hsp70 like the ATP-competitive inhibitor **VER-155008** or allosteric ATPase activity inhibitor **MKT-077**. .

2.3. Binding mode evaluation of S1g-6

A docking simulation was carried out to predict the binding mode of **S1g-6** in complex of Hsp70. As shown in the top-ranked binding mode (Fig. 3), **S1g-6** could be well-positioned into the hydrophobic Bim-binding groove on the surface of the nucleotide-binding domain (NBD) of Hsp70. The cyclohexylthiol group (R_1) of **S1g-6** occupied the deepest hydrophobic pocket at the bottom of the groove, which is consistent with the fact that compounds with hydrophobic thiophenol or cycloalkyl thiol group as R_1 showed better binding affinity than others (Table 1). The 2-carboxyl group located adjacent to residues T226 and H227 on Hsp70 NBD domain, the key residues for Bim binding [20], may form H-bonds with them (distance < 3.5 Å). The morpholine group (R_2) of **S1g-6**

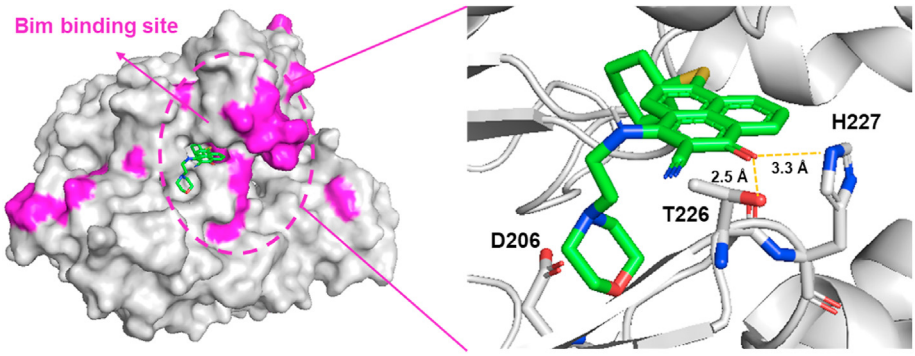

Fig. 3. Predicted binding models of **S1g-6** in complex with Hsp70 (PDB:5AZQ) by docking simulation. Residues with significant chemical shift or peak intensity changes upon Bim binding in TROSY-HSQC assays [20] were shown in pink color.

pointed to the side chain -COOH group of D206 in Hsp70, explaining why compounds with hydrophilic R_2 groups exhibited enhanced binding capability.

2.4. Validation of the target specificity of S1g-6 in situ

Firstly, we carried out a large-scale chemoproteomics experiment to assess the potential targets of **S1g-6** in whole human cell proteome by affinity-based protein profiling. **S1g-6** was incorporated with a well-established "minimalist" linker to generate the affinity-based probe, **S1g-6-probe**, which was synthesized according to published methods (Scheme 2). **S1g-6-probe** was added to CML cell line BV173 cells lysate in the presence or absence of the corresponding competitor **S1g-6**, and then the **S1g-6-probe**-binding targets were pulled down from lysate together with this probe by streptavidin-modified agarose beads. LC-MS/MS analysis revealed 170 proteins (Supplementary Data S1), and these candidates were further analyzed by corresponding volcano plots as statistical significance $\log_{10}$ (p-value) of **S1g-6-probe** enriched proteins against ($\log_2$) of competition ratio (**S1g-6-probe** with excess competitor **S1g-6**) via iTRAQ-based quantitative intensity test. In this assay, only Hsp70 and its homologs, Hsc70 and Mortalin, showed enrichment $\log_{10}$ (p-value) ratios and $\log_2$(**S1g-6**/vehicle) higher than the significance criterion (>2, Fig. 4a), illustrating that **S1g-6** selectively targets Hsp70 in the proteome. This result was further validated by pull-down/western blotting (WB) experiments with **S1g-6-probe** and the Hsp70/Hsc70/Mortalin antibody, which showed that these Hsp70 family proteins were efficiently enriched by **S1g-6-probe** and competed in a concentration-dependent manner with **S1g-6** (Fig. 4b). Taken together, it can be concluded that Hsp70 family proteins are the specific target of **S1g-6** in living cells and **S1g-6** exhibits similar binding capacities toward Hsp70, Hsc70, and Mortalin.

Next, the single-turnover ATPase rates assay showed **S1g-6** selectively inhibits the co-chaperone function of Bim to activate the ATPase activity of Hsc70, rather than directly suppress the overall ATPase activity of Hsc70, just like it did to Hsp70 (Fig. 4c). Further, the capability and selectivity of **S1g-6** to target Hsp70-Bim PPI in living cells were confirmed by co-immunoprecipitation (co-IP) experiments (Fig. 4d). We tested the perturbation of Hsp70-Bim in BV173 cell line upon treatment with **S1g-6**, **VER-155008**, and **MKT-077**, at a gradient of concentrations (0, 1, 3, and 5 μM). The Hsp70-Bag3 (a co-chaperone exhibiting different binding site with Bim) complex [19], the target of **MKT-077** and its analogies [12,13], was tested in parallel. As expected, **VER-155008** failed to disrupt both Hsp70-Bim and Hsp70-Bag3 interactions, while **MKT-077** interfered with Hsp70-Bag3 PPI. Notably, **S1g-6** dose-dependently inhibited the Hsp70-Bim complex and showed no obvious impact on the Hsp70-Bag3 complex even at the highest concentration, which validated that **S1g-6** specifically targets the Hsp70-Bim PPI. **MKT-077** exhibited a much weaker Hsp70-Bim PPI disruption.

It is reasonable for **MKT-077** to disturb Hsp70-Bim PPI because its binding site is near the Bim binding site, while **VER-155008** binds far from it. The Hsp70-Bim PPI disruption in cells by the three molecules are consistent with their IC_{50} values to disrupt Hsp70-Bim PPI *in vitro* as shown in Table 1.

We can't exclude that the other reported Hsp70 inhibitors could also interfere with Hsp70-Bim PPI even though they bind apart from the Bim binding site, because allosteric effects may be involved. However, **S1g-6** could exhibit the most potent and reliable targeting toward Hsp70-Bim both *in vitro* and *in situ* so far.

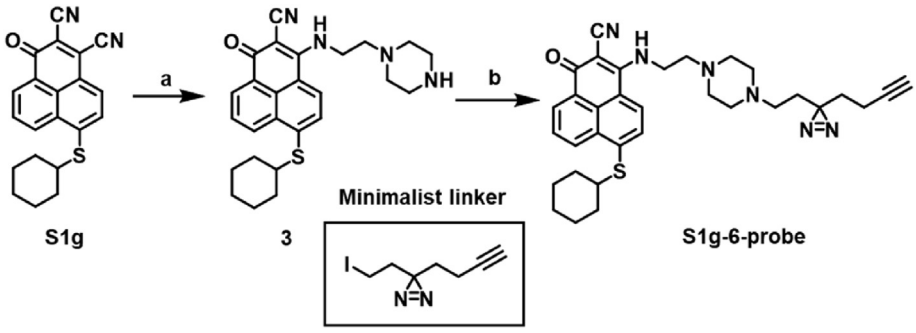

Scheme 2. Chemical structure and synthetic route of **S1g-6-probe**. Reagents and conditions: (a) 2-(piperazin-1-yl) ethan-1-amine, CH_3CN, rt, 2 h. (b) Minimalist linker, K_2CO_3, DMF, 60 °C, 4 h.

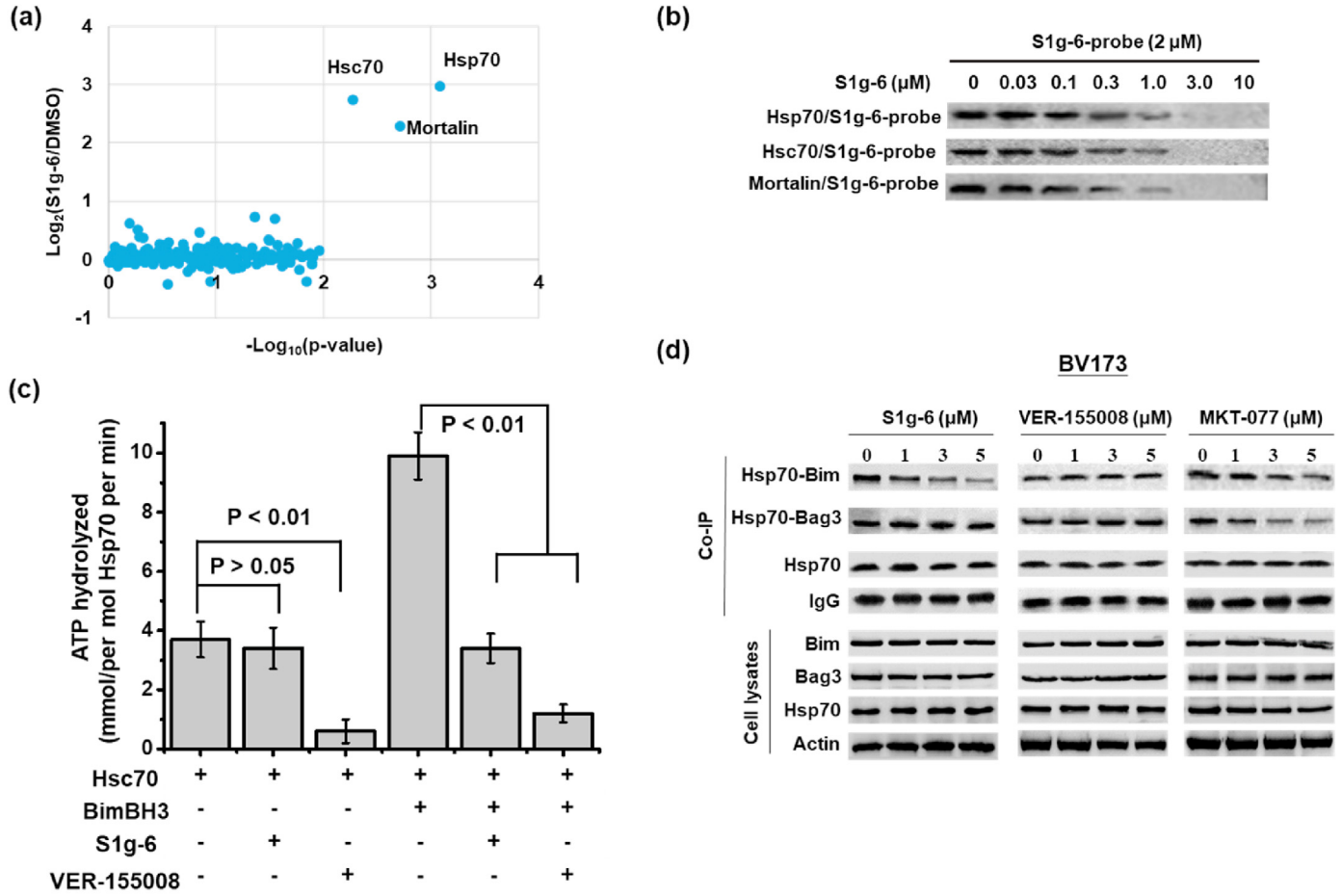

Fig. 4. (a) Volcano plots as statistical significance (log_{10}p-value) of **S1g-6-probe** enriched proteins against (log_2) of competition ratio (**S1g-6-probe** with excess competitor **S1g-6**) via iTRAQ-based quantitative intensity test in BV173 cell lysates. (b) Assays of the competitive binding of **S1g-6** to Hsp70/Hsc70/Mortalin-**S1g-6-probe** complexes in cell lysates determined by Western blot. (c) ATPase activity of Hsp70 treated with BimBH3, **S1g-6** and **VER-155008**. Error bars show the mean ± s.e.m. (n = 3). (d) Western blot and Co-IP analysis of the levels of Hsp70, Bim, Bag3 and their PPIs in BV173 cells upon treatment with a gradient of concentrations (0–5 μM) of **S1g-6**, **VER-155008** and **MKT-077**, respectively, using β-actin as a loading control. All figures represent the results from n = 3 independent samples.

2.5. Identification of the anti-cancer molecular biological mechanism of S1g-6

To investigate whether the specific Hsp70-Bim PPI inhibitor **S1g-6** could induce the selective killing effect for cancer cells over normal tissue cells, we analyzed the apoptosis induction of **S1g-6** in CML cell lines BV173 and KCL22, and normal tissue cell lines HEK293 and BaF3. **VER-155008** and **MKT-077** was used as control. These cell lines were chosen because Hsp70-Bim PPI was found to stabilize oncogenic clients and suppress apoptosis in BV173 and KCL22 cell lines. As shown in Table 2, **VER-155008** and **MKT-077** exhibited broad-spectrum killing activity over all these cells (EC_{50} = 5.5–8.7 μM and 2.7–6.6 μM). On the contrary, **S1g-6** potently induced apoptosis in BV173 and KCL22 (EC_{50} = 1.42 and 2.60 μM), and exhibited no obvious cytotoxic effect in HEK293 and BaF3 (EC_{50} > 15 μM), showing much lower toxicity towards normal cells than **VER-155008** and **MKT-077**. This result also validated the discovery in our previous work that co-chaperone Bim helps Hsp70 recognize some cancer-related clients, making some cancer cells addict to Hsp70-Bim function [20]. Moreover, **S1g-6** showed higher killing activity in BV173 and KCL22 than the ATP-competitive inhibitor **VER-155008**. Despite the explanation that nanomolar concentrations of Bim is much easier to be competed from Hsp70 than millimolar concentrations of ATP in the cytosol, the higher antitumor efficiency of **S1g-6** than **VER-155008** further suggested a cancer-related role of Hsp70-Bim.

Next, we investigated the transduction signal pathway that Hsp70-Bim PPI inhibitor **S1g-6** induced in cancer cells. In our previous study, we identified that the Hsp70-Bim PPI regulates the fold of oncogenic clients AKT and Raf-1 in cancer cells to suppress apoptosis [20]. Herein, treatment of BV173 and KCL22 cells with **S1g-6** significantly decreased the expression and phosphorylation

Table 2
The EC_{50} value of **S1g-6** and **VER-155008** for apoptosis induction in cancer and normal tissue cells determined by Annexin V staining.

Compounds	BV173 EC_{50} (μM)	KCL22 EC_{50} (μM)	HEK293 EC_{50} (μM)	BaF3 EC_{50} (μM)
S1g-6	1.4 ± 0.2	2.6 ± 0.4	>15	>15
VER-155008	5.5 ± 1.9	6.8 ± 1.1	8.7 ± 1.2	6.1 ± 1.7
MKT-077	2.7 ± 0.3	3.2 ± 0.4	6.6 ± 0.6	5.4 ± 0.4

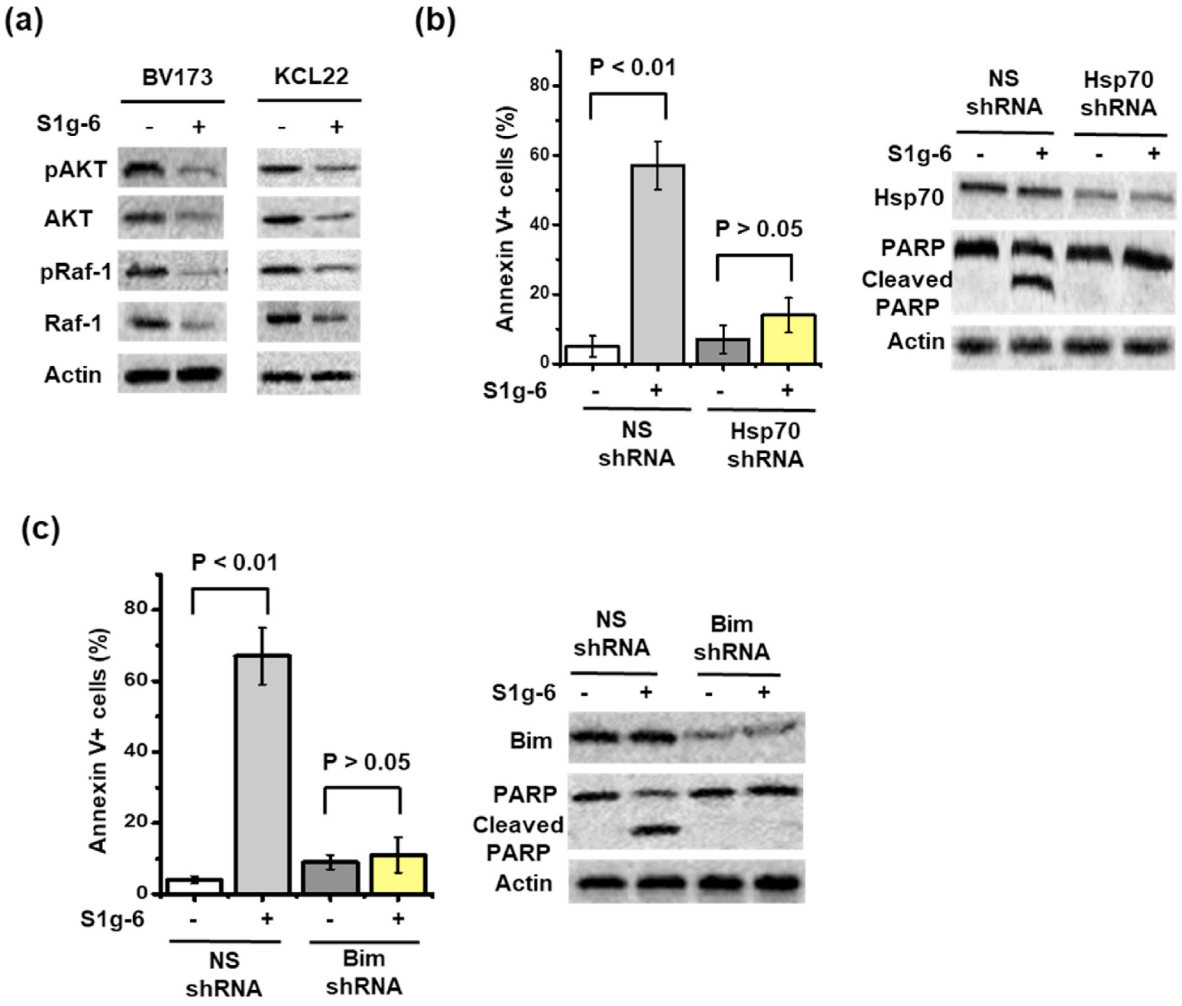

Fig. 5. (a) Western blot analysis of the levels of AKT, Raf-1, pAKT and pRaf-1 in BV173 and KCL22 cell lines upon treatment with **S1g-6** (3 μM), using β-actin as a loading control. (b) **S1g-6** (3 μM) induced apoptosis in stable clones from NS/Hsp70 shRNA-transfected BV173 cells determined by Annexin V staining and Western blot showing PARP cleavage. (c) **S1g-6** (3 μM) induced apoptosis in stable clones from NS/Bim shRNA-transfected BV173 cells determined by Annexin V staining and Western blot showing PARP cleavage. Figures represent the results from n = 3 independent samples, and the data are expressed as the mean ± s.e.m. (n = 3).

levels of AKT and Raf-1, illustrating the capacity of **S1g-6** to perturb the Hsp70-Bim function in living cells (Fig. 5a).

Further, the dependency of Hsp70-Bim complex in **S1g-6**-induced apotosis was validated through cell-based shRNA assays. As shown in Fig. 5b and c, stable clones from both Hsp70 shRNA-transfected and Bim shRNA-transfected cells showed obvious resistance to **S1g-6**-induced apoptosis which is indicated by Annexin V staining and PARP cleavage.

3. Conclusion

Taken together, through derivation, screening, and optimization of **S1**, a small molecular BimBH3 mimetic developed by our group, we discovered a novel Hsp70 inhibitor, **S1g-6,** which exhibited sub-μM binding affinity toward Hsp70 and selectively disrupted Hsp70-Bim PPI. The target specificity of **S1g-6** *in situ* was validated by affinity-based protein profiling, co-immunoprecipitation, and cell-based shRNA assays, which demonstrated that **S1g-6**-induced apoptosis completely depends on disrupting Hsp70-Bim PPI. **S1g-6** selectively induced apoptosis in cancer cell lines over normal cell lines, making it a completely new class of Hsp70 inhibitor and a promising antitumor candidate. Additionlly, validation of a new cancer therapeutic target, Hsp70-Bim PPI, is emergeing to discriminate the cancer-related Hsp70 functions and otherwise.

4. Experimental section

4.1. Chemistry

All commercial reagents were purchased and used without further purification unless otherwise stated. ^{1}H NMR spectra were obtained with a Bruker AV-500 spectrometer with chemical shifts reported as ppm (in DMSO, TMS as an internal standard). Mass spectra were obtained on a HPLC-Q-Tof MS (Micro) spectrometer. Column chromatography was performed on silica gel 200−300 mesh. The purity of all final products was determined by analytical HPLC to be ≥ 95%. HPLC purity of compounds was measured with a normal-phase HPLC (XBridge C18, 4.6 mm × 150 mm, 5 μm) with two diverse wavelength detection systems.

4.2. General procedure for the synthesis of compounds S1-S1i

In a round-bottom flask, a mixture of acenaphthequinone (1.0 equiv) and malononitrile (1.1 equiv) were stirred in CH_3CN at 65 °C for 3 h. The resulting mixture was cooled to rt, and then filtered to give the desired product **1**. The crude product was used for next

step without further purification.

In a round-bottom flask, a mixture of **1** (1.0 equiv) and K_2CO_3 (0.1 equiv) were stirred in CH_3CN at 65 °C for 3 h. The resulting mixture was cooled to rt, filtered, and washed for 3 times using CH_3CN and H_2O, respectively. The expected product compound **2** was isolated as an orange powder, with yield = 45% over two steps.

To a suspension of compound **2** (1.0 equiv) in CH_3CN, corresponding R_1H (4.0 equiv) was added at rt, and the mixture was further stirred at 60 °C for 3 h. Then, the solvent was removed under reduced pressure, and the crude was purified on silica gel (Hexane:CH_2Cl_2:EA = 30:30:1) to give the expected product **S1-S1i**, with yield = 36−55%, respectively.

4.2.1. 1-Oxo-6-thiomorpholino-1H-phenalene-2,3-dicarbonitrile (S1)

Purple powder, yield = 41%. ^{1}H NMR (500 MHz, $CDCl_3$): δ 8.77 (d, J = 7.7 Hz, 1H), 8.48 (d, J = 8.3 Hz, 1H), 8.24 (d, J = 8.0 Hz, 1H), 7.87 (t, J = 8.4 Hz, 1H), 7.20 (d, J = 8.1 Hz, 1H), 3.78 (t, J = 4.8 Hz, 4H), 2.99 (t, J = 4.5 Hz, 4H). ^{13}C NMR (125 MHz, $CDCl_3$): δ 175.2, 155.1, 139.7, 131.7, 131.4, 129.3, 127.8, 126.5, 122.6, 120.5, 118.6, 115.8, 114.9, 55.6, 24.8. ESI-MS: m/z for $C_{19}H_{14}N_3OS$ $[M+H]^+$, calc 332.09, found 332.07.

4.2.2. 6-Phenylthio-1-oxo-1H-phenalene-2,3-dicarbonitrile (S1a)

Red powder, yield = 48%. ^{1}H NMR (500 MHz, $CDCl_3$): δ 8.81 (d, J = 8.1 Hz, 1H), 8.76 (d, J = 8.0 Hz, 1H), 7.83 (t, J = 8.4 Hz, 1H), 7.77 (t, J = 8.3 Hz, 1H), 7.51-7.36 δ (m, 5H), 7.20 (d, J = 8.2 Hz, 1H). ^{13}C NMR (125 MHz, $CDCl_3$): δ 175.5, 139.5, 138.8, 135.7, 134.1, 131.6, 131.2, 129.3, 128.7, 128.2, 127.4, 126.1, 125.0, 120.4, 119.1, 115.5. ESI-MS: m/z for $C_{21}H_{11}N_2OS$ $[M+H]^+$, calc 339.05, found 339.05.

4.2.3. 6-(4-bromophenylthio)-1-oxo-1H-phenalene-2,3-dicarbonitrile (S1b)

Red powder, yield = 45%. ^{1}H NMR (500 MHz, DMSO-d_6): δ 8.66 (t, J = 8.2 Hz, 2H), 8.48 (t, J = 8.1 Hz, 1H), 7.88 (t, J = 8.0 Hz, 1H), 7.70 (d, J = 8.8 Hz, 2H), 7.56 (t, J = 8.1 Hz, 1H), 7.38 (d, J = 8.6 Hz, 2H). ^{13}C NMR (125 MHz, $CDCl_3$): δ 175.1, 140.2, 138.5, 134.7, 131.4, 131.0, 132.7, 131.4, 130.5, 128.8, 128.1, 126.2, 124.7, 121.8, 119.8, 117.6, 114.5. ESI-MS: m/z for $C_{21}H_{10}N_2OSBr$ $[M+H]^+$, calc 416.96, found 416.94.

4.2.4. 6-(4-Isopropylthiophenol)-1-oxo-1H-phenalene-2,3-dicarbonitrile (S1c)

Red powder, yield = 52%. ^{1}H NMR (500 MHz, $CDCl_3$): δ 8.87 (d, J = 8.0 Hz, 1H), 8.82 (d, J = 8.2 Hz, 1H), 8.21 (d, J = 8.3 Hz, 1H), 8.06 (t, J = 8.1 Hz, 1H), 7.56 (d, J = 8.4 Hz, 2H), 7.43 (d, J = 8.4 Hz, 2H), 7.06 (d, J = 8.4 Hz, 1H), 3.03 (m, 1H), 1.33 (d, J = 4.9 Hz, 6H). ^{13}C NMR (125 MHz, $CDCl_3$): δ 176.1, 148.2, 139.6, 138.8, 134.4, 132.8, 131.9, 131.3, 130.7, 128.4, 127.8, 126.1, 125.3, 124.5, 124.1, 118.6, 115.3, 33.6, 24.2. ESI-MS: m/z for $C_{24}H_{17}N_2OS$ $[M+H]^+$, calc 381.10, found 381.09.

4.2.5. 6-(4-methoxyphenylthio)-1-oxo-1H-phenalene-2,3-dicarbonitrile (S1d)

Orange powder, yield = 36%. ^{1}H NMR (500 MHz, $CDCl_3$): δ 8.72 (d, J = 8.1 Hz, 1H), 8.63 (d, J = 8.0 Hz, 1H), 7.77 (t, J = 8.0 Hz, 2H), 7.62 (d, J = 8.4 Hz, 2H), 7.34 (d, J = 8.4 Hz, 2H), 7.24 (d, J = 8.1 Hz, 1H), 3.76 (s, 3H). ^{13}C NMR (125 MHz, $CDCl_3$): δ 175.4, 159.2, 139.9, 138.6, 134.5, 132.2, 131.7, 128.7, 128.1, 127.6, 126.1, 124.8, 120.1, 118.7, 115.2, 114.6, 60.0. ESI-MS: m/z for $C_{22}H_{13}N_2O_2S$ $[M+H]^+$, calc 369.06, found 369.10.

4.2.6. 6-((2-hydroxyethyl)amino)-1-oxo-1H-phenalene-2,3-dicarbonitrile (S1e)

Orange powder, yield = 41%. ^{1}H NMR (500 MHz, DMSO-d_6): δ 8.97 (d, J = 8.1 Hz, 1H), 8.64 (d, J = 8.3 Hz, 1H), 8.03 (d, J = 8.4 Hz, 1H), 7.92 (t, J = 8.2 Hz, 1H), 7.07 (d, J = 8.4 Hz, 1H), 4.47 (t, J = 4.4 Hz, 2H), 3.60 (t, J = 4.6 Hz, 2H). ^{13}C NMR (125 MHz, $CDCl_3$): δ 175.0, 145.6, 144.8, 140.1, 139.1, 134.7, 131.9, 129.9, 127.8, 126.9, 124.7, 124.1, 120.5, 118.6, 114.9, 113.1, 111.2. ESI-MS: m/z for $C_{17}H_{12}N_3O_2$ $[M+H]^+$, calc 290.09, found 290.08.

4.2.7. 6-(cyclopentylthio)-1-oxo-1H-phenalene-2,3-dicarbonitrile (S1f)

Red powder, yield = 50%. ^{1}H NMR (500 MHz, $CDCl_3$): δ 8.76 (d, J = 8.0 Hz, 1H), 8.74 (t, J = 7.8 Hz, 2H), 7.78 (t, J = 8.0 Hz, 1H), 7.54 (d, J = 8.1 Hz, 1H), 3.54 (q, J = 4.4 Hz, 1H), 1.70-1.42 δ (m, 8H). ^{13}C NMR (125 MHz, $CDCl_3$): δ 175.7, 140.0, 139.2, 134.7, 131.9, 131.2, 128.4, 127.7, 124.7, 121.9, 120.6, 117.9, 115.6, 45.2, 33.8, 26.8. ESI-MS: m/z for $C_{20}H_{15}N_2OS$ $[M+H]^+$, calc 331.09, found 331.06.

4.2.8. 6-(cyclohexylthio)-1-oxo-1H-phenalene-2,3-dicarbonitrile (S1g)

Red powder, yield = 55%. ^{1}H NMR (500 MHz, $CDCl_3$): δ 8.52 (d, J = 8.0 Hz, 1H), 8.29 (d, J = 8.1 Hz, 1H), 8.23 (d, J = 8.0 Hz, 1H), 7.80 (t, J = 8.1 Hz, 1H), 7.52 (d, J = 7.8 Hz, 1H), 3.55 (q, J = 4.6 Hz, 1H), 2.14 (t, J = 4.3 Hz, 2H), 1.78 (t, J = 4.4 Hz, 2H), 1.61-1.46 δ (m, 6H). ^{13}C NMR (125 MHz, $CDCl_3$): δ 175.1, 139.8, 138.6, 134.5, 131.8, 131.1, 129.6, 128.6, 127.4, 124.8, 121.6, 120.2, 118.3, 115.8, ESI-MS: m/z for $C_{21}H_{17}N_2OS$ $[M+H]^+$, calc 345.10, found 345.09.

4.2.9. 6-(benzylamino)-1-oxo-1H-phenalene-2,3-dicarbonitrile (S1h)

Dark pink powder, yield = 54%. ^{1}H NMR (500 MHz, DMSO-d_6): δ 9.08 (d, J = 8.1 Hz, 1H), 8.72 (d, J = 7.9 Hz, 1H), 8.03 δ (m, 2H), 7.43 (d, J = 8.4 Hz, 2H), 7.38 (t, J = 8.3 Hz, 2H), 7.30 (t, J = 8.6 Hz, 1H), 7.02 (d, J = 8.0 Hz, 1H), 4.88 (s, 2H). ^{13}C NMR (125 MHz, $CDCl_3$): δ 175.3, 139.8, 137.4, 131.8, 131.2, 128.5, 127.5, 126.8, 126.2, 125.1, 123.0, 120.2, 119.3, 118.2, 115.6, 108.5, 47.9. ESI-MS: m/z for $C_{22}H_{14}N_3O$ $[M+H]^+$, calc 336.10, found 336.11.

4.2.10. 6-(cyclohexylamino)-1-oxo-1H-phenalene-2,3-dicarbonitrile (S1i)

Dark pink powder, yield = 52%. ^{1}H NMR (500 MHz, DMSO-d_6): δ 9.23 (d, J = 8.0 Hz, 1H), 8.71 (d, J = 7.8 Hz, 1H), 8.01 (d, J = 8.1 Hz, 1H), 7.97 (t, J = 7.8 Hz, 1H), 7.18 (d, J = 8.0 Hz, 1H), 3.93 (m, J = 4.0 Hz, 1H), 2.03 (d, J = 4.2 Hz, 2H), 1.83 (d, J = 4.1 Hz, 2H), 1.70 (d, J = 4.4 Hz, 1H), 1.57 (q, J = 4.1 Hz, 2H), 1.45 (q, J = 4.0 Hz, 2H), 1.21 (q, J = 4.1 Hz, 2H). ^{13}C NMR (125 MHz, $CDCl_3$): δ 175.2, 151.1, 139.8, 131.8, 131.4, 131.0, 127.7, 128.8, 125.2, 122.8, 120.1, 118.8, 118.0, 115.4, 108.8, 61.5, 32.9, 26.1, 25.2. ESI-MS: m/z for $C_{21}H_{18}N_3O$ $[M+H]^+$, calc 328.14, found 328.11.

4.3. General procedure for the synthesis of compounds S1g-1~S1g-6

To a suspension of compound **S1g** (1.0 equiv) in CH_3CN, corresponding R_2H (30 equiv) was added at rt, and the mixture was further stirred at rt for 6 h. Then, the solvent was removed under reduced pressure, and the crude was purified on silica gel (CH_2Cl_2:CH_3OH = 100:1-20:1) to give the expected product **S1g-1~S1g-6**, with yield = 12−21%, respectively. The major by-product is the 6-R_2 substitution product, for thiol group is a better leaving group than cyan group.

4.3.1. 3-(benzylamino)-6-(cyclohexylthio)-1-oxo-1H-phenalene-2-carbonitrile (S1g-1)

Yellow powder, yield = 14%. ^{1}H NMR (500 MHz, $CDCl_3$): δ 8.64 δ (m, 3H), 8.18 (t, J = 8.1 Hz, 1H), 8.08 (t, J = 8.3 Hz, 1H), 7.78 (d, J = 8.4 Hz, 1H), 7.71-7.64 δ (m, 3H), 5.14 (d, J = 7.8 Hz, 2H), 3.34 δ (m, 1H), 2.01 (d, J = 4.3 Hz, 2H), 1.76 (t, J = 4.5 Hz, 4H), 1.65 (t, J = 4.2 Hz, 4H). ^{13}C NMR (125 MHz, $CDCl_3$): δ 177.6, 175.7, 138.4, 137.0, 134.1,

132.5, 131.9, 131.2, 128.8, 128.3, 127.8, 126.2, 125.7, 124.8, 124.3, 124.0, 123.7, 115.8, 78.3, 53.3, 48.4, 34.2, 25.6, 25.6. ESI-MS: *m/z* for $C_{27}H_{25}N_2OS$ $[M+H]^+$, calc 425.17, found 425.18.

4.3.2. 3-((cyclohexylmethyl)amino)-6-(cyclohexylthio)-1-oxo-1H-phenalene-2-carbonitrile (S1g-2)

Yellow powder, yield = 15%. ^{1}H NMR (500 MHz, $CDCl_3$): δ 8.56 (t, *J* = 8.4 Hz, 2H), 8.19 (d, *J* = 8.1 Hz, 1H), 7.77 (t, *J* = 8.0 Hz, 1H), 7.71 (t, = 8.3 Hz, 1H), 3.86 (d, *J* = 4.6 Hz, 2H), 3.38 (q, *J* = 4.1 Hz, 1H), 2.09 (d, *J* = 4.4 Hz, 2H), 1.76-1.69 δ (m, 10H), 1.68-1.55 δ (m, 4H), 1.55-1.47 δ (m, 5H). ^{13}C NMR (125 MHz, $CDCl_3$): δ 177.4, 175.1, 137.6, 134.4, 132.5, 131.8, 130.8, 128.1, 127.7, 124.7, 124.2, 123.9, 115.7, 78.3, 53.3, 38.7, 34.1, 26.1, 25.3. ESI-MS: *m/z* for $C_{27}H_{31}N_2OS$ $[M+H]^+$, calc 431.22, found 431.25.

4.3.3. 3-(butylamino)-6-(cyclohexylthio)-1-oxo-1H-phenalene-2-carbonitrile (S1g-3)

Yellow powder, yield = 21%. ^{1}H NMR (500 MHz, DMSO-d_6): δ 8.62 (d, *J* = 7.8 Hz, 1H), 8.54 (t, *J* = 8.0 Hz, 1H), 8.48 (d, *J* = 8.1 Hz, 1H), 7.79 δ (m, 2H), 4.27 (t, *J* = 4.4 Hz, 2H), 3.68 δ (m, 1H), 2.08 δ (m, 5H), 1.76 (t, *J* = 4.4 Hz, 2H), 1.63 (t, *J* = 4.2 Hz, 1H), 1.51-1.30 δ (m, 6H), 0.96 (t, *J* = 4.1 Hz, 3H). ^{13}C NMR (125 MHz, DMSO-d_6): δ 177.2, 175.6, 137.8, 134.0, 131.9, 131.7, 131.1, 128.4, 127.3, 124.2, 123.8, 123.4, 115.9, 78.1, 53.4, 42.8, 34.4, 33.0, 25.6, 25.3, 20.4, 13.8. ESI-MS: *m/z* for $C_{24}H_{27}N_2OS$ $[M+H]^+$, calc 391.18, found 391.21.

4.3.4. 6-(cyclohexylthio)-3-((2-hydroxyethyl)amino)-1-oxo-1H-phenalene-2-carbonitrile (S1g-4)

Yellow powder, yield = 15%. ^{1}H NMR (500 MHz, DMSO-d_6): δ 8.45 (d, *J* = 8.7 Hz, 1H), 8.24 (d, *J* = 8.4 Hz, 1H), 8.14 (d, *J* = 8.5 Hz, 1H), 7.74 (d, *J* = 8.3 Hz, 1H), 7.69 (t, *J* = 8.1 Hz, 1H), 4.30 (t, *J* = 5.7 Hz, 2H), 4.14 (t, *J* = 5.4 Hz, 2H), 3.46 δ (m, 1H), 2.00 (d, *J* = 4.4 Hz, 2H), 1.74 (d, *J* = 4.3 Hz, 2H), 1.58 (d, d, *J* = 3.9 Hz, 1H), 1.46-1.33 δ (m, 4H), 1.25 δ (m, 2H). ^{13}C NMR (125 MHz, DMSO-d_6): δ 177.2, 175.5, 138.1, 134.3, 132.2, 131.7, 131.0, 128.2, 127.5, 124.6, 124.1, 123.6, 115.8, 78.3, 56.4, 53.3, 46.7, 34.3, 25.8, 25.4. ESI-MS: *m/z* for $C_{22}H_{23}N_2O_2S$ $[M+H]^+$, calc 379.15, found 379.13.

4.3.5. 3-((2-cyano-6-(cyclohexylthio)-1-oxo-1H-phenalen-3-yl) amino)propanamide (S1g-5)

Yellow powder, yield = 12%. ^{1}H NMR (500 MHz, DMSO-d_6): δ 8.58 (d, *J* = 7.8 Hz, 1H), 8.49 (d, *J* = 7.6 Hz, 1H), 8.46 (t, *J* = 7.7 Hz, 1H), 7.81 δ (m, 2H), 4.11 (t, *J* = 6.1 Hz, 2H), 3.80 (t, *J* = 5.8 Hz, 2H), 3.65 δ (m, 1H), 2.02 (t, *J* = 4.3 Hz, 2H), 1.75 (t, *J* = 4.5 Hz, 2H), 1.62 δ (m, 1H), 1.43 δ (m, 4H), 1.26 δ (m, 3H). ^{13}C NMR (125 MHz, DMSO-d_6): δ 177.6, 175.1, 174.4, 138.4, 134.1, 132.1, 131.5, 131.0, 128.4, 127.6, 124.8, 124.4, 124.0, 115.7, 78.2, 53.4, 40.4, 38.2, 34.1, 25.7, 25.3. TOF ESI-MS: *m/z* for $C_{23}H_{24}N_3O_2S$ $[M+H]^+$, calc 406.52, found 406.51.

4.3.6. 6-(cyclohexylthio)-3-((2-morpholinoethyl)amino)-1-oxo-1H-phenalene-2-carbonitrile (S1g-6)

Yellow powder, yield = 14%. ^{1}H NMR (500 MHz, DMSO-d_6): δ 8.56 (d, *J* = 8.4 Hz, 1H), 8.42 (d, *J* = 8.2 Hz, 1H), 8.29 (d, *J* = 8.1 Hz, 1H), 7.84 δ (m, 2H), 4.02 (t, *J* = 4.4 Hz, 2H), 3.73 δ (m, 1H), 3.57 (t, *J* = 6.4 Hz, 4H), 3.03 δ (m, 4H), 2.75 (t, *J* = 4.7 Hz, 2H), 2.04 δ (m, 2H), 1.75 (t, *J* = 4.6 Hz, 2H), 1.61 δ (m, 1H), 1.29-1.23 δ (m, 5H). ^{13}C NMR (125 MHz, DMSO-d_6): δ 178.1, 175.4, 138.8, 134.8, 132.1, 131.3, 128.4, 127.4, 124.8, 124.1, 123.5, 115.9, 78.6, 66.6, 56.1, 54.5, 53.2, 40.6, 34.3, 25.9, 25.1. ESI-MS: *m/z* for $C_{26}H_{30}N_3O_2S$ $[M+H]^+$, calc 448.21, found 448.18.

4.4. Procedure for the synthesis of compounds S1g-6-probe

To a suspension of compound **S1g** (1.0 equiv) in CH_3CN, 2-(piperazin-1-yl)ethan-1-amine (30 equiv) was added at rt, and the mixture was further stirred at rt for 6 h. Then, the solvent was removed under reduced pressure, and the crude was purified on silica gel (CH_2Cl_2:CH_3OH = 20:1) to give the expected product **3**, with yield = 14%.

To a suspension of compound **3** (1.0 equiv) in DMF, the minimalist linker (1.1 equiv) and K_2CO_3 (3.0 equiv) were added at rt. Then, the mixture was stirred at 60 °C for 4 h, and the solvent was removed under reduced pressure. The crude was purified on silica gel (CH_2Cl_2:CH_3OH = 30: 1) to give the expected product **S1g-6-probe**, with yield = 77%.

4.4.1. 3-((2-(4-(2-(3-(but-3-yn-1-yl)-3H-diazirin-3-yl)ethyl) piperazin-1-yl)ethyl)amino)-6-(cyclohexylthio)-1-oxo-1H-phenalene-2-carbonitrile. (S1g-6-probe)

^{1}H NMR (500 MHz, DMSO-d_6): δ 8.59 (d, *J* = 8.2 Hz, 1H), 8.46 (d, *J* = 7.8 Hz, 1H), 8.41 (d, *J* = 7.9 Hz, 1H), 7.89 (t, *J* = 8.1 Hz, 1H), 7.54 (d, *J* = 8.2 Hz, 1H), 4.13 (q, *J* = 6.7 Hz, 2H), 3.46 δ (m, 8H), 2.92 (t, *J* = 6.4 Hz, 2H), 2.76 (s, 1H), 2.63 (t, *J* = 6.2 Hz, 2H), 2.26 (t, *J* = 5.4 Hz, 2H), 2.05 (t, *J* = 4.6 Hz, 2H), 1.81 δ (m, 5H), 1.74 (t, *J* = 4.4 Hz, 3H), 1.72-1.53 δ (m, 5H), 1.25 δ (m, 4H). ^{13}C NMR (500 MHz, DMSO-d_6): δ 175.2, 173.3, 171.1, 138.7, 134.9, 131.4, 131.3, 128.2, 127.7, 124.8, 124.4, 123.1, 115.8, 98.0, 83.7, 70.0, 68.7, 58.0, 53.4, 47.4, 45.0, 34.2, 33.0, 30.1, 28.0, 25.9, 25.3, 11.2. ESI-MS: *m/z* for $C_{33}H_{39}N_4OS$ $[M + H-N_2]^+$, calc 539.29, found 539.27.

4.5. Protein expression and purification

Constructs of hHsp70 NBD (1−383), hHsc70 NBD (1−383) and hBcl-2 (2−206) cDNA were subcloned into the pHis vector, and the resulting proteins with an N-terminal 6 × His tag were produced in Escherichia coli strain BL21 (DE3) containing the corresponding plasmid. The samples were produced in LB medium. The proteins were further purified by Sephadex G-75 size exclusion chromatography (GE Healthcare), before they were pooled and concentrated for biochemical or structural assays.

4.6. Fluorescence polarization assays (FPAs)

A mixture of 10 nM FAM-labeled BimBH3 peptide and 300 nM Bcl-2 (2−206) or Hsp70 NBD (1−383) protein was preincubated in the assay buffer (100 mM potassium phosphate, pH 7.5; 100 μg/mL bovine gamma globulin; 0.02% sodium azide). Next, serial dilutions of compounds were added. After a 30 min incubation, the polarization values were measured using the Spectra Max M5 Detection System in a black 96-well plate. The polarization value was plotted as a function of the concentration of the compound, and the IC_{50} value was determined from the competitive inhibition curve.

4.7. Isothermal titration calorimetry (ITC)

The Hsp70 NBD (1−383)-compound (**S1g-6/MKT-077**) and Hsc70 NBD (1−383)-compound (**S1g-6/MKT-077**) interactions were characterized at 25 °C using ITC200 (GE Healthcare/MicroCal). A typical experiment included the injection of 13 aliquots containing approximately 0.2 mM ligand solution into a protein solution of approximately 20 μM in the ITC cell (in a total volume of approximately 200 μL). An additional set of injections was run in a separate experiment with buffer instead of the protein solution as a control. Before data analysis, the control values were subtracted from the main experimental data.

The Origin 7.0-based software provided by GE/MicroCal was used for data analysis. The binding isotherms were integrated to give the enthalpy change (ΔH), plotted as a function of the molar ratio of the ligand. The ΔH/molar ratio plot was a sigmoidal,

representing the fractional saturation of the binding sites by the ligand, and therefore the one set of sites model was used as the basic option. The dissociation constant K_d was determined from the slope of the central linear part of the fractional saturation curve.

4.8. Molecular docking

The 3D structures of the human Hsp70 NBD (Hsp70; PDB 5AZQ) were obtained from the RCSB Protein Data Bank. The 3D structures of the inhibitors were generated using Chembio3D Ultra 11.0 followed by energy minimization. The AutoDock 4.0 program equipped with ADT was used to perform the automated molecular docking. Grid maps covering residues that were perturbed by more than the threshold value of 0.1 ppm on the Hsc70 protein surface were defined for all inhibitors in the AutoDock calculations using a grid spacing of 0.6 Å. The GA-LS algorithm was adopted using default settings, and 100 hybrid GA-LS runs were carried out. A total of 100 possible binding conformations were generated and grouped into clusters based on a 1.0 Å cluster tolerance. The docking models were analyzed and represented using ADT.

4.9. Cell lines, reagents and chemical inhibitors

Cell lines were purchased from American Type Culture Collection and used within 6 months from resuscitation. KCL22 and BV-173 were cultured in RPMI 1640 medium (Thermo Scientific HyClone, Beijing, China). HEK-293T cells were cultured in DMEM medium (Thermo Scientific HyClone, Beijing, China). BaF3 cells were cultured in RPMI 1640 medium with 10 ng/ml mouse IL-3 (R&D Systems, Minneapolis, MN, USA). All of medium were supplemented with 10% heat inactivated fetal bovine serum (FBS; Gibco BRL, Grand Island, NY, USA) and 100 U/mL penicillin-streptomycin and all cells were cultured at 37 °C and 5% CO_2. **VER-155008** was purchased from Selleck Chemicals (Shanghai, China), and **MKT-077** was purchased from MedChem Express (Monmouth Junction, NJ, USA), all the chemicals were dissolved in dimethylsulfoxide (DMSO) to a concentration of 10 mM. To obtain the final concentration, stock solutions were diluted in culture medium.

4.10. Affinity-based protein profiling (AfBPP)

Cells were grown to 80–90% confluency in 24-well plates under conditions described above. The medium was removed, and cells were washed twice with cold PBS and then treated with 0.5 mL of the DMEM-containing probe (diluted from DMSO stocks whereby DMSO never exceeded 1% in the final solution). After 5 h of incubation (37 °C, 5% CO_2), the medium was aspirated, and cells were washed gently with PBS (2 ×) to remove excessive probe, followed by UV irradiation for 20 min on ice. The cells were trypsinized and pelleted by centrifugation. The cell pellets were resuspended in PBS (50 μL), homogenized by sonication, and diluted to 1 mg/mL with PBS.

One microliter of a freshly premixed click chemistry reaction cocktail in PBS (2.5 mM Biotin-N_3 from 10 mM stock solution in DMSO, 2.5 mM TBTA from 10 mM freshly prepared stock solution in deionized water, 25 mM TCEP from 100 mM freshly prepared stock solution in deionized water, and 25 mM $CuSO_4$ from 100 mM freshly prepared stock solution in deionized water) was added. The reaction was further incubated for 2 h with gentle mixing, before being terminated by addition of prechilled acetone (0.5 mL; 30 min incubation at −20 °C). Precipitated proteins were subsequently collected by centrifugation (13000 rpm × 10 min at 4 °C), resolubilized in 1% SDS in 50 μL of PBS and then incubated with avidin-agarose beads (100 μL/mg of protein) at 4 °C overnight. After centrifugation, the supernatant was removed. The beads were washed with 0.1% SDS once and PBS four times and then boiled in SDS loading buffer (2 ×) [200 mM Tris, 400 mM dithiothreitol (DTT), and 8% SDS, pH 6.8] for 15 min.

4.11. iTRAQ-based quantitative proteomic profiling of the interactome

For LC-MS/MS protein identification, above pull-down fractions were separated by SDS-10% polyacrylamide gels, followed by Coomassie blue staining. Each lane was cut into multiple gel slices. Trypsin digestion was performed on each gel slice with an in-gel trypsin digestion kit (Pierce). The resulting peptide mixtures were desalted and loaded onto an Acclaim PePmap C18-reversed phase column (75 μm × 2 cm, 3 μm, 100 Å thermo scientific) and separated with reversed phase C18 column (75 μm × 10 cm, 5 μm, 300 Å, Agela Technologies) mounted on a Dionex ultimate 3000 nano LC system. Peptides were eluted using a gradient of 5–80% (v/v) acetonitrile in 0.1% formic acid over 45 min at a flow rate of 300 nL min-1 combined with a Q Exactive mass spectrometer (Thermo Fisher Scientific, MA, USA). The eluates were directly entered Q-Exactive MS (Thermo Fisher Scientific, Waltham, MA, USA), setting in positive ion mode and data-dependent manner with full MS scan from 350 to 2000 m/z, full scan resolution at 70,000, MS/MS scan resoltion at 17,500. MS/MS scan with minimum signal threshold 1E+5, isolation width at 2 Da. To evaluate the performance of this mass spectrometry on the iTRAQ labeled samples, two MS/MS acquisition modes, higher collision energy dissociation (HCD) was employed. And to optimize the MS/MS acquisition efficiency of HCD, normalized collision energy (NCE) was systemically examined, stepped 20%.

4.12. Annexin V-FITC staining assay for apoptosis

Phosphatidylserine exposure was quantified by surface Annexin V-FITC staining. Cells were treated with inhibitor in 48 h and then transferred from a culture well (1.2 × 10^6/well) to a tube and washed with PBS containing 1% (v/v) bovine calf serum (Hyclone, Logan, UT, USA). According to the manufacturer's instructions, the cells were incubated with a 1:40 solution of FITC-conjugated Annexin V (Roche Diagnostics, Germany) in the dark for 10 min at room temperature and the Annexin V-FITC positive cells were analyzed by flow cytometry on a BD FACSCalibur (BD Biosciences, Becton Drive, Franklin Lakes, NJ, USA). Cell Questc software (BD Biosciences) was used to determine the percentage of apoptosis in the samples. (The inhibition concentration 50 (IC_{50}) was defined as the concentration of the drug required to induce apoptosis by 50%.)

4.13. Immunoblotting

Cells were either treated with inhibitor or DMSO (vehicle) and lysed in RIPA buffer (Solarbio, Beijing, China) supplementing Halt protease/phosphatase inhibitor cocktail (Pierce Biotechnology, Rockford, USA) for 30 min on ice and centrifuged at 12,000 g for 15 min at 4 °C. Protein concentrations were determined using BCA assay (Beyotime, Shanghai, China) according to the manufacturer's instructions. Lysates (150–250 μg) were electrophoretically resolved by SDS-PAGE, transferred to PVDF membrane and probed with the following primary antibodies against: Hsp70 (1:1000, 10995-1-AP; Proteintech), Bag-3 (1:1000, 10599-1-P; Proteintech), Bim (1:1000, 2933; CST), PARP (1:500, sc-8007; Santa Cruz Biotechnology), AKT (1:800, PAB1310; Abnova), Raf-1 (1:800, PAB26752; Abnova), pAKT (1:5000, ab81283; Abcam), pRaf-1 (1:1000, ab173539; Abcam), Actin (1:10000, A01010; Abbkine). Immune complexes were visualized by the use of Super Signal West

Pico Chemiluminescent Substrate (Pierce Biotechnology) and detected on a Kodak Image Station 4000 MM Pro (New Haven, CT, USA).

4.14. Co-immunoprecipitation (co-IP)

Cells were washed twice with ice cold PBS and lysed on ice in IP-buffer (10 mM HEPES, pH 7.4, 50 mM NaCl, 5 mM $MgCl_2$, 1 mM EGTA, 5% glycerol, 0.5% Triton X-100) supplemented with 1% protease/phosphatase inhibitor for 30 min. After centrifugation (15 min, 12,000 g, 4 °C), supernatants were collected and normalized to the protein content. 2 μg of antibody were added to an input volume of 200 μl with 5–10 mg/ml protein. As control IPs were done with same amounts of purified rabbit or mouse IgG (Thermo Fisher, Scientific). After shaking overnight at 4 °C, 20 μl protein G sepharose beads (GE Healthcare, Madison, WI, USA) were added and the samples incubated for 2 h at 4 °C with constant rotation. Immunocomplexes were washed three times with IP buffer and solved by heating for 5 min at 95 °C by immunoblotting analysis.

Declaration of competing interest

The authors declare that they have no known competing financial interests or personal relationships that could have appeared to influence the work reported in this paper.

Acknowledgments

This research was supported by the National Natural Science Foundation of China (81903462 and 82073703), the China Postdoctoral Science Foundation (2018M641694) and the Fundamental Research Funds for the Central Universities (DUT20LK28 and DUT20YG133).

Appendix A. Supplementary data

Supplementary data to this article can be found online at https://doi.org/10.1016/j.ejmech.2021.113452.

Data and materials availability

All data needed to evaluate the conclusions in the paper are present in the paper and/or the Supplementary Materials. Additional data related to this paper may be requested from the authors.

References

[1] M.E. Murphy, The HSP70 family and cancer, Carcinogenesis 34 (2013) 1181–1188.
[2] M.Y. Sherman, V.L. Gabai, Hsp70 in cancer: back to the future, Oncogene 34 (2015) 4153–4161.
[3] G.D. Lianos, G.A. Alexiou, A. Mangano, A. Mangano, S. Rausei, L. Boni, G. Dionigi, D.H. Roukos, The role of heat shock proteins in cancer, Canc. Lett. 360 (2015) 114–118.
[4] J. Wu, T. Liu, Z. Rios, Q. Mei, X. Lin, S. Cao, Heat shock proteins and cancer, Trends Pharmacol. Sci. 38 (2017) 226–256.
[5] F.U. Hartl, A. Bracher, M. Hayer-Hartl, Molecular chaperones in protein folding and proteostasis, Nature 475 (2011) 324–332.
[6] W.B. Pratt, J.E. Gestwicki, Y. Osawa, A.P. Lieberman, Targeting Hsp90/Hsp70-based protein quality control for treatment of adult onset neurodegenerative diseases, Annu. Rev. Pharmacol. Toxicol. 55 (2015) 353–371.
[7] C.L. Klaips, G.G. Jayaraj, F.U. Hartl, Pathways of cellular proteostasis in aging and disease, J. Cell Biol. 217 (2018) 51–63.
[8] B. Rodriguez-Iturbe, M.A. Lanaspa, R.J. Johnson, The role of autoimmune reactivity induced by heat shock protein 70 in the pathogenesis of essential hypertension, Br. J. Pharmacol. 176 (2019) 1829–1838.
[9] L. Shrestha, H.J. Patel, G. Chiosis, Chemical tools to investigate mechanisms associated with HSP90 and HSP70 in Disease, Cell Chem. Biol. 23 (2016) 158–172.
[10] M. Ferraro, I. D'Annessa, E. Moroni, G. Morra, A. Paladino, S. Rinaldi, F. Compostella, G. Colombo, Allosteric Modulators of HSP90 and HSP70: dynamics meets function through structure-based drug design, J. Med. Chem. 62 (2019) 60–87.
[11] J.E. Gestwicki, H. Shao, Inhibitors and chemical probes for molecular chaperone networks, J. Biol. Chem. 294 (2019) 2151–2161.
[12] X. Li, S.R. Srinivasan, J. Connarn, A. Ahmad, Z.T. Young, A.M. Kabza, E.R.P. Zuiderweg, D. Sun, J.E. Gestwicki, Analogues of the allosteric heat shock protein 70 (Hsp70) inhibitor, MKT-077, as anti-cancer agents, ACS Med. Chem. Lett. 4 (2013) 1042–1047.
[13] H. Shao, X. Li, M.A. Moses, L.A. Gilbert, C. Kalyanaraman, Z.T. Young, M. Chernova, S.N. Journey, J.S. Weissman, B. Hann, M.P. Jacobson, L. Neckers, J.E. Gestwicki, Exploration of benzothiazole rhodacyanines as allosteric inhibitors of protein-protein interactions with heat shock protein 70 (Hsp70), J. Med. Chem. 61 (2018) 6163–6177.
[14] D.M. Huryna, J.L. Brodskyc, K.M. Brummonda, P.G. Chambersa, B. Eyera, A.W. Irelandc, M. Kawasumid, M.G. LaPortea, K. Lloyda, B. Manteaua, P. Nghiemd, B. Quadea, S.P. Seguinc, P. Wipf, Chemical methodology as a source of small-molecule checkpoint inhibitors and heat shock protein 70 (Hsp70) modulators, Proc. Natl. Acad. Sci. Unit. States Am. 108 (2011) 6757–6762.
[15] A. Rodina, P.D. Patel, Y. Kang, Y. Patel, I. Baaklini, M.J.H. Wong, T. Taldone, P. Yan, C. Yang, R. Maharaj, A. Gozman, M.R. Patel, H.J. Patel, W. Chirico, H. Erdjument-Bromage, T.T. Talele, J.C. Young, G. Chiosis, Identification of an allosteric pocket on human Hsp70 reveals a mode of inhibition of this therapeutically important protein, Chem. Biol. 20 (2013) 1469–1480.
[16] D.V. Sverchinsky, A.D. Nikotina, E.Y. Komarova, E.R. Mikhaylova, N.D. Aksenov, V.F. Lazarev, V.A. Mitkevich, R. Suezov, D.S. Druzhilovskiy, V.V. Poroikov, B.A. Margulis, I.V. Guzhova, Etoposide-induced apoptosis in cancer cells can Be reinforced by an uncoupled link between Hsp70 and caspase-3, Int. J. Mol. Sci. 19 (2018) 2519–2534.
[17] S.-K. Ko, J. Kim, D.C. Na, S. Park, S.-H. Park, J.Y. Hyun, K.-H. Baek, N.D. Kim, N.-K. Kim, Y.N. Park, K. Song, I. Shin, A small molecule inhibitor of ATPase activity of HSP70 induces apoptosis and has antitumor activities, Chem. Biol. 22 (2015) 391–403.
[18] M.A. Mikeladze, E.A. Dutysheva, V.G. Kartsev, B.A. Margulis, I.V. Guzhova, V.F. Lazarev, Disruption of the complex between GAPDH and Hsp70 sensitizes C6 glioblastoma cells to hypoxic stress, Int. J. Mol. Sci. 22 (2021) 1520–1535.
[19] T.A. Colvin, V.L. Gabai, J.L. Gong, S.K. Calderwood, H. Li, S. Gummuluru, O.N. Matchuk, S.G. Smirnova, N.V. Orlova, I.A. Zamulaeva, M. Garcia-Marcos, X. Li, Z. Young, J.N. Rauch, J.E. Gestwicki, S. Takayama, M.Y. Sherman, Hsp70-Bag3 interactions regulate cancer-related signaling networks, Canc. Res. 74 (2014) 4731–4740.
[20] Z. Guo, T. Song, Z. Wang, D. Lin, K. Cao, P. Liu, Y. Feng, X. Zhang, P. Wang, F. Yin, J. Dai, S. Zhou, Z. Zhang, The chaperone Hsp70 is a BH3 receptor activated by the pro-apoptotic Bim to stabilize anti-apoptotic clients, J. Biol. Chem. 295 (2020) 12900–12909.
[21] Z. Zhang, G. Wu, F. Xie, T. Song, X. Chang, 3-Thiomorpholin-8-oxo-8H-acenaphtho[1,2-b]pyrrole-9-carbonitrile (S1) based molecules as potent, dual inhibitors of B-cell lymphoma 2 (Bcl-2) and myeloid cell leukemia sequence 1 (Mcl-1): structure-based design and structure-activity relationship studies, J. Med. Chem. 54 (2011) 1101–1105.
[22] T. Song, Q. Chen, X. Li, G. Chai, Z. Zhang, Correction to 3-Thiomorpholin-8-oxo-8H-acenaphtho[1,2-b]pyrrole-9-carbonitrile (S1) based molecules as potent, dual inhibitors of B-cell lymphoma 2 (Bcl-2) and myeloid cell leukemia sequence 1 (Mcl-1): structure-based design and structure-activity relationship studies, J. Med. Chem. 56 (2013) 9366–9367.
[23] D.S. Williamson, J. Borgognoni, A. Clay, Z. Daniels, P. Dokurno, M.J. Drysdale, N. Foloppe, G.L. Francis, C.J. Graham, R. Howes, A.T. Macias, J.B. Murray, R. Parsons, T. Shaw, A.E. Surgenor, L. Terry, Y.K. Wang, M. Wood, A.J. Massey, Novel adenosine-derived inhibitors of 70 kDa heat shock protein, discovered through structure-based design, J. Med. Chem. 52 (2009) 1510–1513.
[24] A. Rousaki, Y. Miyata, U.K. Jinwal, C.A. Dickey, J.E. Gestwicki, E.R.P. Zuiderweg, Allosteric drugs: the interaction of antitumor compound MKT-077 with human HSP70 chaperones, J. Mol. Biol. 411 (2011) 614–632.
[25] A.J. Souers, J.D. Leverson, E.R. Boghaert, S.L. Ackler, N.D. Catron, J. Chen, B.D. Dayton, H. Ding, S.H. Enschede, W.J. Fairbrother, D.C.S. Huang, S.G. Hymowitz, S. Jin, S.L. Khaw, P.J. Kovar, L.T. Lam, J. Lee, H.L. Maecker, K.C. Marsh, K.D. Mason, M.J. Mitten, P.M. Nimmer, A. Oleksijew, C.H. Park, C.M. Park, D.C. Phillips, A.W. Roberts, D. Sampath, J.F. Seymour, M.L. Smith, G.M. Sullivan, S.K. Tahir, C. Tse, M.D. Wendt, Y. Xiao, J.C. Xue, H.C. Zhang, R.A. Humerickhouse, S.H. Rosenberg, S.W. Elmore, ABT-199, a potent and selective BCL-2 inhibitor, achieves antitumor activity while sparing platelets, Nat. Med. 19 (2013) 202–208.